Three-loop contributions to $b \to s\gamma$ associated with the current-current operators

Christoph Greub[a], Hrachia M. Asatrian[b], Hrachya H. Asatryan[c],
Lukas Born[a] and Julian Eicher[a]

[a] *Albert Einstein Center for Fundamental Physics, Institute for Theoretical Physics, University of Bern, CH-3012 Bern, Switzerland*

[b] *Yerevan Physics Institute, 0036 Yerevan, Armenia*

[c] *Yerevan State University, 0070 Yerevan, Armenia*

Abstract

In a recent work, we calculated all three-loop diagrams contributing to the decay amplitude for $b \to s\gamma$ where none of the gluons touch the b-leg. In the present paper, we complete the calculation by working out all remaining three-loop diagrams (of order α_s^2) associated with the current-current operators O_1 and O_2 at the physical value of the charm-quark mass m_c. Using the programs `AMFlow` and `DiffExp` to solve the differential equations for the master integrals, we obtained precise numerical results at 23 values for $z = m_c^2/m_b^2$, ranging from $z = 1/1000$ to $z = 1/5$, along with asymptotic expansions around $z = 0$. For certain diagrams, the asymptotic expansion breaks down in the physical z-range, necessitating a Taylor expansion (which we do around $z = 1/10$). In all expansions, we retained power terms up to z^{20} and included the accompanying $\log(z)$ terms to all powers for asymptotic expansions. Numerical results for the sum of all diagrams (including those calculated in the previous paper) are presented in tabular form, while the mentioned expansions of individual diagram classes are provided electronically. We note that our results for the asymptotic expansions around $z = 0$ are in good agreement with those recently published by Fael *et al.* and Czaja *et al.*.

1 Introduction

Rare B-meson decays have been the focus point of theorists and experimentalists for some time, due to the potential to test the Standard Model (SM) at scales of several hundreds of GeV. The decay $B \to X_s \gamma$ is particularly suitable as it allows a very stringent comparison of experimental and theoretical information. Both experiment and theory have made substantial progress over the last two decades and have already reached an impressive precision which puts strong constraints on extensions of the SM. In view of further increasing precision for the experimental measurements, refined theoretical predictions are required. This is possible because the (inclusive) decay $B \to X_s \gamma$ can be approximated by the quark-level process $b \to X_s \gamma$ which can be treated by perturbative QCD in the effective theory obtained after integrating out the heavy particles t, W, Z and H.

At the present or expected precision of the experimental measurements of the decay $B \to X_s \gamma$, a full next-to-next-to-leading logarithmic order (NNLL) calculation is necessary to reduce the theoretical uncertainties and to make a rigorous comparison with existing and future experimental data.

A first estimate of the branching ratio at NNLL level, leading to $\mathcal{B}(B \to X_s \gamma) = (3.15 \pm 0.23) \times 10^{-4}$, was done in [1]. An updated version for this branching ratio, incorporating those results for NNLL contributions and lower-order perturbative corrections that had been calculated after 2006, was provided in [2] where some of us were involved. The CP- and isospin-averaged branching ratio reads $\mathcal{B}(B \to X_s \gamma) = (3.36 \pm 0.23) \times 10^{-4}$ which is in agreement with the current experimental average $\mathcal{B}(B \to X_s \gamma) = (3.49 \pm 0.19) \times 10^{-4}$ given in [3]. We note that all of these numbers refer to a cut of the photon energy below 1.6 GeV.

A sizeable part of the uncertainty in [2] is due to the fact that so far there is no exact calculation with the correct mass for the charm quark m_c at NNLL order. Instead, the results are obtained via interpolation, i.e., by using the results obtained through the large m_c asymptotic expansion on one hand and the results for $m_c = 0$ on the other hand. An improvement resulted from calculating a limited set of diagrams with closed fermion loops on gluon lines at order α_s^2 for the physical value of m_c in [4][1]; see also [5–7]. Let us remind the reader that the complete NNLL calculation of the branching ratio includes a large number of diagrams associated with different effective operators, which pose their own difficulties that have to be overcome.

We feel that the time has come to close the gap on m_c. In [8] we started the computation of virtual α_s^2 corrections to the decay amplitude $b \to s\gamma$ associated with the current-current operators, that is the matrix elements of these operators. We worked out all those diagrams where no gluons are touching the b-quark line. These contributions, which we denote in the following as "s-leg diagrams", are shown in Figure 1 of [8]. We also set out to calculate the

---

[1]The diagrams calculated are those occurring in the interference of the current-current and photonic dipole operators.

remaining diagrams[2].

A few months later, two papers were published [9, 10] in which our results were confirmed and extended to the complete set of virtual correction diagrams. As these highly non-trivial computations are ingredients in the NNLL program which need checking, we decided to continue an independent calculation of the contributions which were not included in our paper [8]. To this end, we evaluate in the present paper all diagrams of order α_s^2 in Figure 1 where no gluon touches the s-quark line (referred to as "b-leg diagrams"), as well as the "mixed diagrams" in Figure 2, and finally the "bubble diagrams" in Figure 3 where the gluon propagator is dressed by a fermion-, a gluon- or a ghost-loop.

The remainder of this paper is organized as follows: In Section 2 we present the theoretical framework and a few conventions. In Section 3 we present the methodology of solving differential equations using the program `AMFlow`, as well as checks we have done using the program `DiffExp`. In Section 4, we present numerical results for $z \doteq m_c^2/m_b^2 = 0$ and at 23 points between $z = 1/1000$ and $z = 1/5$. We also provide the result as an asymptotic expansion around $z = 0$ (which contains non-negative integer and half-integer powers of z as well as non-negative integer powers of $\log(z)$). As it turns out that this expansion breaks down in the physical $z-$range for some "b-leg" diagrams, we also provide a Taylor expansion for this class around the value $z = 1/10$ (which is a typical physical value for z). We illustrate with a plot that the transition between the two mentioned formulas is very smooth. We note that the authors of [9] also worked out several expansions; they explicitly gave the result for the asymptotic expansion around $z = 0$, which is in perfect agreement with our formula. In Section 5 we summarize our work. The results for different classes of diagrams are submitted in electronic form together with the paper, as described in the Appendix.

2 Theoretical framework

B-meson or b-quark decay amplitudes are usually calculated within the Weak Effective Theory (WET) where the SM particles with EW-scale masses have been integrated out. The WET Lagrangian then contains QCD and QED interactions, and a tower of higher dimensional local operators which is typically truncated at dimension six [15, 16]. The part of the WET Lagrangian which is relevant for the contributions discussed in this paper is

$$\mathcal{L}_{\text{WET}} = \mathcal{L}^{(4)} + \frac{4G_F}{\sqrt{2}} V_{ts}^* V_{tb} \Big[C_1 O_1 + C_2 O_2 + C_7 O_7 \Big], \tag{2.1}$$

---

[2]This work can be considered as an extension of our work [11], where the corresponding α_s^1 corrections were calculated.

where

$$O_1 = (\bar{s}\gamma_\mu P_L T^a c)(\bar{c}\gamma^\mu P_L T^a b) \ , \qquad\qquad O_2 = (\bar{s}\gamma_\mu P_L c)(\bar{c}\gamma^\mu P_L b) \ ,$$

$$O_7 = \frac{e}{16\pi^2} m_b(\mu)(\bar{s}\sigma_{\mu\nu} P_R b) F^{\mu\nu} \ . \tag{2.2}$$

$\mathcal{L}^{(4)}$ contains the usual kinetic terms and the mass terms of the quarks u, d, s, c, b as well as their interactions with the photon and the gluons. $P_{R,L} = (1 \pm \gamma_5)/2$ stand for the right and left projection operator, $\sigma_{\mu\nu} \equiv (i/2)[\gamma_\mu, \gamma_\nu]$ and our convention for the covariant derivative is given by $D_\mu q = (\partial_\mu + ieQ_q A_\mu + ig_s T^A G_\mu^A)q$; $m_b(\mu)$ in the definition of O_7 denotes the mass of the b-quark in the $\overline{\text{MS}}$-scheme. Note that what is calculated in this paper are only the bare (i.e. unrenormalized) α_s^2 corrections from $O_{1,2}$ to the decay amplitude for $b \rightarrow s\gamma$. In these terms the renormalization scheme of m_b and m_c is not fixed (scheme differences would result in effects of $O(\alpha_s^3)$). Furthermore, we will neglect the strange quark mass throughout our paper.

2.1   Form factor decomposition

As mentioned in some detail in [8], the decay amplitude $\mathcal{A}(b \rightarrow s\gamma) = \langle s\gamma|O_{1,2}|b\rangle$ can be written as $\mathcal{A} = M_\mu \, \varepsilon^\mu$, where ε^μ denotes the polarization vector of the emitted photon. In the considered limit where the strange quark mass is put to zero, M_μ is of the form

$$M_\mu = \bar{u}_s(p_s) P_R \left[A\, q_\mu + B\, p_\mu + C\, \gamma_\mu \right] u_b(p) \ . \tag{2.3}$$

In this equation $u_b(p)$ denotes the Dirac spinor of the b-quark with four-momentum p, $u_s(p_s)$ is the analogous quantity for the s-quark with four-momentum p_s and $q = p - p_s$ is the four-momentum of the emitted photon. Applying standard algebraic manipulations, the form factors A, B, C are given in terms of linear combinations of scalar three-loop integrals[3]. After performing these integrals and taking into account that $q^2 = 0$ in our process, these form factors are functions of m_b and m_c (and depend also on the renormalization scale μ). The function A does not contribute to $b \rightarrow s\gamma$ since the corresponding tensor structure vanishes when contracting M_μ with the polarization vector. Furthermore, the Ward identity $q^\mu M_\mu = 0$ (resulting from electromagnetic gauge invariance) implies that

$$C = -\frac{m_b}{2}\, B \, . \tag{2.4}$$

This Ward identity for on-shell amplitudes, derived in detail for instance in sections 7.4 and 10 of the text-book by Peskin and Schroeder [17], holds for renormalized amplitudes in which the masses of external particles are defined in the on-shell scheme. In our present paper, we only calculate the bare version of the form factor B. When later including the renormalization

---

[3]The form of such integrals can be seen e.g. in Eq. (3.4) in our previous paper [8].

of the amplitude, we suggest to calculate the effects of the counterterms on B only and then *use* the relation (2.4) to get the renormalized version of C. This procedure à priori leads to expressions for renormalized form factors B and C in the on-shell scheme for m_b. By performing a further appropriate finite renormalization, one can transform the form factors to any other renormalization scheme for m_b.

Two remarks concerning the diagrams leading to the bare version of the form factor B are in order, which are best illustrated in Figure 1 of [8]: first, it is quite easy to see that those diagrams which are marked with a cross that does not carry a number would only contribute to the form factor C. Therefore only the diagrams with numbered crosses (1-44) had to be worked out. Second, diagrams which contain a 1-loop quark self-energy on the very left or very right of the external b- or s-leg (i.e. which formally contain a zero propagator denominator) are omitted from the list of bare diagrams; their effects can be taken into account later by quark wave function renormalization. Note that in the present paper we only listed those (numbered) diagrams which contribute to the bare form factor B. For the calculation of this form factor we employ the method of differential equations, which is detailed in Section 3.

2.2 Comment on the computation of bubble diagrams

We note that for the "bubble diagrams" in Figure 3 it is sufficient to calculate only the diagrams where the gluon propagator is dressed by a fermion loop; as has been shown in [12–14], the sum of the ghost- and the gluon-loop can be obtained from the massless fermion loop diagrams by replacing (in the Feynman gauge)

$$n_\ell \, tr \;\to\; -C_A \left(\frac{5}{4} + \frac{\epsilon}{2} + \frac{\epsilon^2}{2} + \frac{\epsilon^3}{2} + O(\epsilon^4) \right) , \tag{2.5}$$

where n_ℓ denotes the number of massless quarks and C_A and tr are color factors.

3 Differential equations

In this section, we explain the details of the calculations of the form factor B using the method of differential equations. The general outline of this method is as follows: express each diagram (or sets of diagrams) as a linear combination of scalar integrals, which in turn are reduced to a smaller number of master integrals (MIs) by applying Integration-By-Parts (IBP) identities to the scalar integrals (see [18–26]). We use the program `Kira` [19] to bring the scalar integrals to a set of MIs. In general, there are many different sets (we can call each set a basis) of MIs we can reduce to. In [23], an algorithm is suggested which chooses a "good" basis in the sense that the ϵ dependence factors out in the denominators of the relations in which the scalar integrals are expressed in terms of MIs; this simplifies further steps in the calculation,
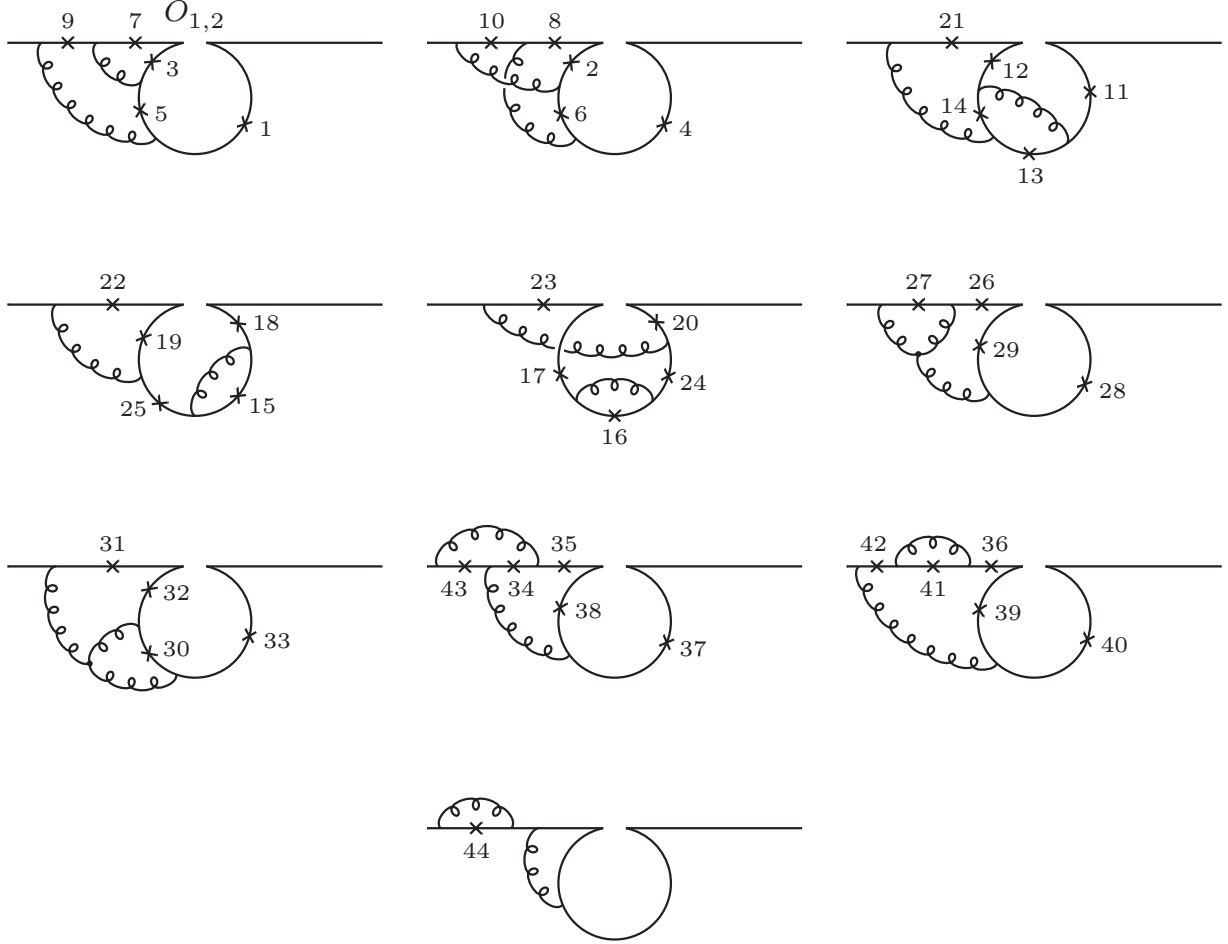
Figure 1: "b-leg diagrams": List of three-loop contributions to $b \to s\gamma$ associated with O_1 and O_2, where no gluon touches the s-leg. A cross on a quark line represents a possible place where the photon can be emitted. Only the diagrams which contribute to the form factor B are shown; they carry a diagram number next to the cross. See also the text at the end of Section 2.1.
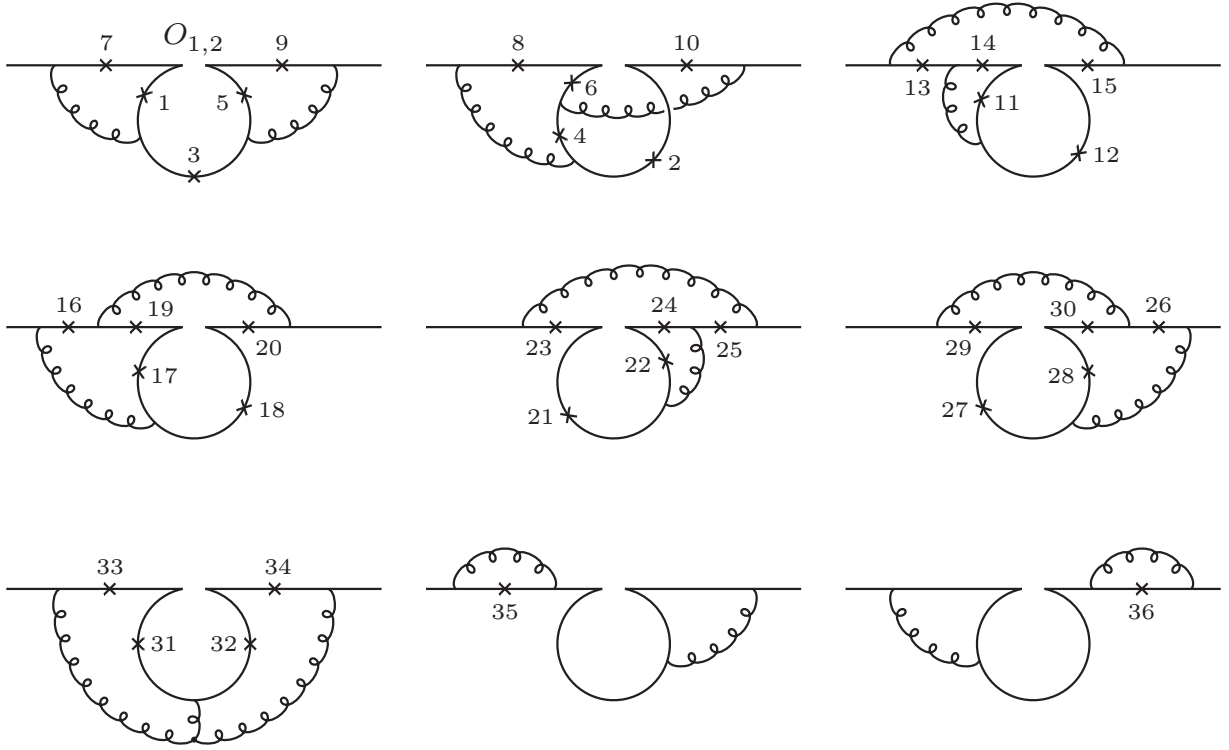
Figure 2: "Mixed diagrams": List of three-loop contributions to $b \to s\gamma$ associated with O_1 and O_2, where one gluon touches the b-leg and one touches the s-leg. A cross on a quark line represents a possible place where the photon can be emitted. Only the diagrams which contribute to the form factor B are shown.
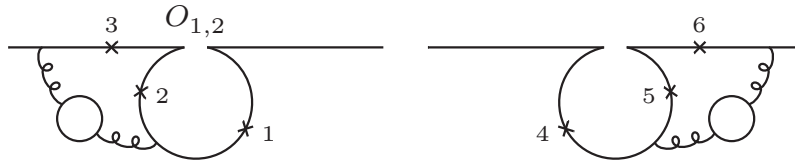

Figure 3: List of the "bubble diagrams" contributing to $b \to s\gamma$ associated with O_1 and O_2. A cross on a quark line represents a possible place where the photon can be emitted. The particle running in the bubble (inserted in the gluon line) is one of the following: a massless fermion (u, d, s-quarks), a fermion with mass m_c, a fermion with mass m_b, a gluon, or a ghost. Only the diagrams which contribute to the form factor B are shown.

in particular solving the differential equations. We therefore use this "good" basis throughout our calculations.

Using the IBP identities generated by `Kira`, one can construct a system of differential equations for the MIs with respect to z. These equations are of the form

$$\partial_z J_k(\epsilon, z) = a^{k\ell}(\epsilon, z) J_\ell(\epsilon, z), \tag{3.1}$$

where $a^{k\ell}$ are the entries of a $N \times N$ matrix depending on ϵ and z. The derivatives of the MIs J_k are obtained by differentiating the integrands, which produce new scalar integrals. These scalar integrals are then subjected to IBP reduction again to express the derivatives $\partial_z J_k$ in terms of the MIs J_ℓ (for more detail, see [8]).

In [8], two methods were used for solving the differential equations. For most diagrams, we were able to transform the differential equation into canonical form [27], where the equations could then be solved in an iterative manner as an expansion in ϵ. The z dependence in these solutions are contained in Generalized Polylogarithms (GPLs) [28]. After fixing the integration constants (using the large m_c behavior of the MIs), we were left with purely analytical precise results. However, for two sets of diagrams (namely (11, 12) and (13, 14)), we were unable to transform the differential equations to canonical form. As such, a different method was used to solve these differential equations: a series expansion was constructed around $z = 0$, by bringing the differential equation matrix first to Fuchsian form [29] and then to Jordan form. This leads to a simple first-order linear differential equation, which has N linearly independent fundamental solutions. To fix the integration constants, the program `FIESTA5` [30] was used. This program allows to numerically calculate the leading terms of the z-expansion of the MIs directly from their integral representations. This entire process is discussed in detail in [8]. The problem with this second approach is the precision of `FIESTA5`; the authors of [9] state that when comparing with the results of our "s-leg diagrams", for the sets of diagrams involving `FIESTA5` results, the agreement was only 5 digits, while for other sets, it was at least 10 digits. Given the extra complexity of the classes of diagrams we solve in the present paper, it is problematic to use the first method (that is, solving the differential equations analytically) for most sets of diagrams, forcing us to use the second method which involves `FIESTA5`. We found, however, that the results suffer from very low precision; therefore we use a different method for the solution of our differential equations, which is discussed in the following subsections.

3.1 Calculation of boundary conditions for differential equations

To solve the system of differential equations for a given diagram in the three classes considered in this paper, we need N boundary conditions, where N is the number of MIs in the diagram. We use the program `AMFlow` [31], which is based on the methods developed in [32], to calculate these boundary conditions at a specific point. In our application `AMFlow` receives as input the value of m_c^2 and m_b^2 (or the value of $z = m_c^2/m_b^2$, when working in units where m_b is put to 1,

as we do), and calculates the given list of master integrals for these values of the quark masses with very high precision as a Laurent series of sufficiently high order in ϵ.

In practice, we used the `AMFlow` package to calculate the boundary values of the MIs at $z = 1/100$.

3.2   Solving the differential equations

To solve the differential equations for a given diagram in the three classes considered in this paper, we use the `DESolver` package of `AMFlow`. `DESolver` allows us to transport the results for the MIs from $z = 1/100$ to any point. We use this functionality to iteratively obtain the results for the MIs at the following 23 points:

$$\left\{ \frac{1}{1000}, \frac{1}{500}, \frac{1}{200}, \frac{1}{100}, \frac{2}{100}, \frac{3}{100}, \frac{4}{100}, \frac{5}{100}, \frac{6}{100}, \frac{7}{100}, \frac{8}{100}, \frac{9}{100}, \right.$$
$$\left. \frac{10}{100}, \frac{11}{100}, \frac{12}{100}, \frac{13}{100}, \frac{14}{100}, \frac{15}{100}, \frac{16}{100}, \frac{17}{100}, \frac{18}{100}, \frac{19}{100}, \frac{20}{100} \right\} \tag{3.2}$$

To validate these results, we also directly calculated the values of the MIs at $z = 1/10$ using `AMFlow`. When comparing the directly calculated values at $z = 1/10$ with those obtained via transportation from $z = 1/100$, we have perfect agreement; this consistency makes us confident that the results for the MIs for each diagram at the 23 points mentioned above are very precise. This in turn also means that we have very precise numerical results for the contribution of the three classes of diagrams to the form factor B (see Eq. (2.3)) at these 23 points.

Besides these numerical results, it is convenient to have also an analytic expression in terms of an asymptotic expansion around $z = 0$ for these contributions to the form factor B. In particular, such an expression also covers the results for the (CKM unsuppressed) u-quark loops in the analogous process $b \to d\gamma$, where the corresponding z is m_u^2/m_c^2, which is basically zero. The asymptotic expansion around $z = 0$ can easily be constructed on a diagram-by-diagram basis with the program `DESolver`, using as input the differential equation matrix, as well as the boundary conditions for the MIs which we have calculated at $z = 1/100$. We worked out this asymptotic expansion for the contribution to the form factor B of all three classes of diagrams. For the "mixed diagrams" and for the "bubble diagrams", the obtained asymptotic formulas coincide very well with the 23 points. Only for "b-leg diagrams", we have noticed that this expansion breaks down within the physical z-range[4]. Detailed investigations show that the convergence radius is not large enough to cover the full relevant z-range for some of the master integrals associated with the diagrams 3-6; this is related to the presence of poles at $z = 1/16$ in certain entries of the matrices which define the differential equations. In Figure

---

[4]We use numerical values $m_c \sim 1.0$ GeV, ..., 1.7 GeV and $m_b \sim 4.2$ GeV, ..., 5.0 GeV which correspond to $z \in [0.04, 0.16]$.
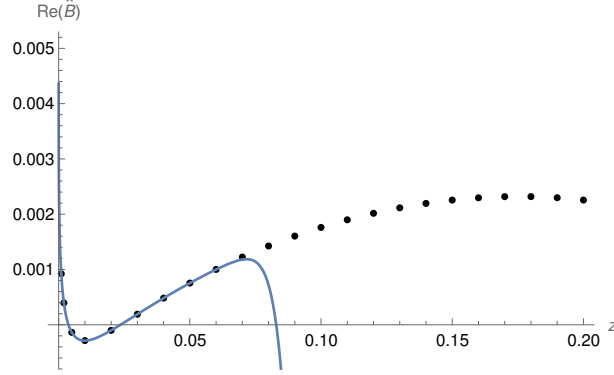
Figure 4: Real part of the ϵ^0 coefficient of the O_2 contribution to $\hat{B}$ as defined in Eq. (4.1). The highlighted points are the 23 points mentioned in the text. The solid line is the sum of the expansion around $z = 0$ for all four classes of diagrams. As can be seen, the asymptotic expansion breaks down around the value of $z = 0.07$.

4, we combine the ϵ^0 coefficients of the three classes of diagrams with the "s-leg diagrams" computed in [8]; the breakdown of the asymptotic expansion is clearly seen. Given that the physical value for z is $\sim 1/10$ (i.e. higher than the value for which the $z = 0$ expansion breaks down), we need a different expansion. To this end, we also worked out a Taylor expansion for the "b-leg diagrams" around $z = 1/10$, which is a regular point of the differential equations; this expansion is also implemented in the `DESolver` package of `AMFlow` and uses as input the values of the MIs at the expansion point. Alternatively, this expansion could also be constructed "by hand": Given the input of the MIs at $z = 1/10$, their first derivatives with respect to z can be obtained at $z = 1/10$ from the right-hand side of eq. (3.1). By interating the differential equation, one also finds the second derivatives at $z = 1/10$, the third derivatives and so on. Having these derivatives at hand, it is straightforward to set up the Taylor expansion. In Figure 5, we illustrate that the transition between these two formulas is very smooth. We therefore propose to give the final results for the "b-leg diagrams" in terms of a "switched expansion", by switching at $z = 0.04$ from the asymptotic expansion to the Taylor expansion, as suggested by the figure. Using these two expansions, we are able to cover all values of z from 0 up to and beyond the physical range. The two expansions are given up to order z^{20} and $(z - 1/10)^{20}$, respectively, after having checked that this accuracy is sufficient. For the asymptotic expansion we have kept the accompanying $\log(z)$ terms to all powers of z. All our results are presented in the electronic file submitted with the paper.

As mentioned at the beginning of this section, the results for "s-leg diagrams" 11-14 in [8] are not very accurate due to limitations of the `FIESTA5` program. Therefore, we have recalculated these four diagrams using our new method. These new calculations are very precise and were used in the final results given in the electronic file submitted with the paper.

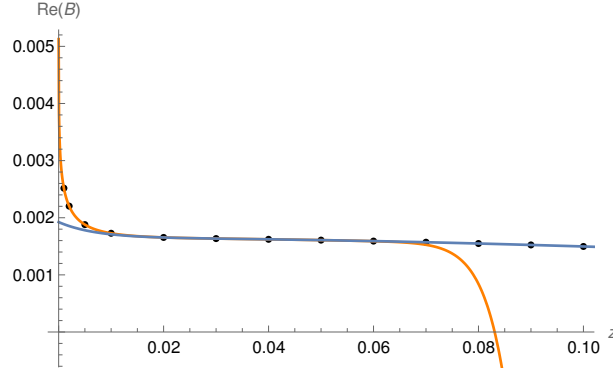Note that we have calculated most of the diagrams also using the program `DiffExp` [33].

Figure 5: Real part of the ϵ^0 coefficient of the O_2 contribution to $\hat{B}$ as defined in Eq. (4.1) for all "b-leg diagrams". The highlighted points are the 23 points mentioned in the text. The orange line shows the sum of the asymptotic expansion for all diagrams in Figure 1, while the blue line shows the corresponding Taylor expansion around $z = 1/10$. The breakdown of the asymptotic expansion near the physical range of z, as well as the breakdown of the Taylor expansion near $z = 0$ are clearly visible. The transition from the asymptotic expansion to the Taylor expansion is very smooth.

4 Results

In this section we present the contributions of all four classes of diagrams of order α_s^2 to the form factor B, both for O_1 and O_2. In fact, we show our results in terms of the dimensionless quantity $\hat{B}$, defined according to

$$B = \text{pref} \cdot \hat{B} \quad \text{with} \quad \text{pref} = -\frac{e\, m_b}{4\pi^2}\, g_s^4 \left(\frac{\mu^2}{m_b^2}\right)^{3\epsilon}. \tag{4.1}$$

In Tables 1 and 2 the dimensionless form factor $\hat{B}$ is given (for all powers of ϵ up to ϵ^0) at the 23 points mentioned in Eq. (3.2) for the operators O_1 and O_2, respectively. We also present the values for $z \to 0$ separately, as the value at this point is not obtained the same way as for the 23 points, but rather from the limit of the asymptotic expansion. We obtain

$$1000 \cdot \hat{B}_{O_1}(0) = -\frac{0.01012}{\epsilon^3} + \frac{0.02486 - 0.02765i}{\epsilon^2} + \frac{0.2802 + 0.09776i}{\epsilon} + (0.6538 + 2.6231i) \tag{4.2}$$

$$1000 \cdot \hat{B}_{O_2}(0) = \frac{0.06073}{\epsilon^3} + \frac{0.08846 + 0.1659i}{\epsilon^2} + \frac{0.2020 + 0.2813i}{\epsilon} + (4.3882 - 5.8342i) \tag{4.3}$$

In Figures 6 and 7 we present the ϵ^0 coefficient's real and imaginary parts of expansions for O_1 and O_2, respectively. Both figures show the "switched expansions" (with switching at $z = 0.04$), as well as the values at the 23 points. The bare form factors $\hat{B}$ associated with the operators O_1 and O_2 have recently been presented in [9][5]. These authors also worked out several expansions; they explicitly gave the result for the asymptotic expansion around $z = 0$,

---

[5]They are denoted there by $t_2^{Q_1}$ and $t_2^{Q_2}$, respectively.

10

O_1	$\frac{1}{\epsilon^2}$	$\frac{1}{\epsilon^1}$	ϵ^0
$\frac{1}{1000}$	$0.02522 - 0.02553i$	$0.3025 + 0.08587i$	$1.278 + 2.269i$
$\frac{1}{500}$	$0.02572 - 0.02425i$	$0.3025 + 0.07716i$	$1.371 + 2.079i$
$\frac{1}{200}$	$0.02716 - 0.02153i$	$0.2936 + 0.05769i$	$1.447 + 1.707i$
$\frac{1}{100}$	$0.02935 - 0.01845i$	$0.2732 + 0.03502i$	$1.432 + 1.325i$
$\frac{2}{100}$	$0.03314 - 0.01437i$	$0.2322 + 0.005243i$	$1.321 + 0.8652i$
$\frac{3}{100}$	$0.03640 - 0.01156i$	$0.1946 - 0.01436i$	$1.200 + 0.5751i$
$\frac{4}{100}$	$0.03931 - 0.009440i$	$0.1602 - 0.02823i$	$1.088 + 0.3689i$
$\frac{5}{100}$	$0.04194 - 0.007765i$	$0.1287 - 0.03832i$	$0.9862 + 0.2139i$
$\frac{6}{100}$	$0.04435 - 0.006405i$	$0.09965 - 0.04568i$	$0.8934 + 0.09385i$
$\frac{7}{100}$	$0.04659 - 0.005284i$	$0.07275 - 0.05097i$	$0.8089 - 0.0005617i$
$\frac{8}{100}$	$0.04867 - 0.004348i$	$0.04775 - 0.05465i$	$0.7317 - 0.07520i$
$\frac{9}{100}$	$0.05062 - 0.003563i$	$0.02447 - 0.05704i$	$0.6612 - 0.1340i$
$\frac{10}{100}$	$0.05245 - 0.002901i$	$0.002748 - 0.05837i$	$0.5967 - 0.1797i$
$\frac{11}{100}$	$0.05418 - 0.002343i$	$-0.01753 - 0.05885i$	$0.5380 - 0.2144i$
$\frac{12}{100}$	$0.05581 - 0.001873i$	$-0.03648 - 0.05863i$	$0.4846 - 0.2397i$
$\frac{13}{100}$	$0.05735 - 0.001479i$	$-0.05419 - 0.05783i$	$0.4365 - 0.2568i$
$\frac{14}{100}$	$0.05881 - 0.001150i$	$-0.07074 - 0.05657i$	$0.3935 - 0.2667i$
$\frac{15}{100}$	$0.06020 - 0.0008767i$	$-0.08619 - 0.05495i$	$0.3556 - 0.2703i$
$\frac{16}{100}$	$0.06151 - 0.0006529i$	$-0.1006 - 0.05305i$	$0.3228 - 0.2684i$
$\frac{17}{100}$	$0.06276 - 0.0004721i$	$-0.1140 - 0.05095i$	$0.2951 - 0.2616i$
$\frac{18}{100}$	$0.06395 - 0.0003285i$	$-0.1266 - 0.04872i$	$0.2725 - 0.2507i$
$\frac{19}{100}$	$0.06508 - 0.0002173i$	$-0.1382 - 0.04643i$	$0.2554 - 0.2362i$
$\frac{20}{100}$	$0.06615 - 0.0001341i$	$-0.1490 - 0.04415i$	$0.2438 - 0.2187i$

Table 1: Dimensionless form factor $1000 \cdot \hat{B}$ of order α_s^2 for the operator O_1, given at the 23 points in Eq. (3.2). The three columns are the coefficients of ϵ^{-2}, ϵ^{-1} and ϵ^0, respectively. The value of the ϵ^{-3} coefficient is z-independent and is equal to -0.01012 for all points.

O_2	$\frac{1}{\epsilon^2}$	$\frac{1}{\epsilon^1}$	ϵ^0
$\frac{1}{1000}$	$0.08632 + 0.1532i$	$0.05402 + 0.2669i$	$0.9238 - 4.765i$
$\frac{1}{500}$	$0.08334 + 0.1455i$	$0.03352 + 0.2671i$	$0.3961 - 4.204i$
$\frac{1}{200}$	$0.07466 + 0.1292i$	$0.02862 + 0.2737i$	$-0.1371 - 3.136i$
$\frac{1}{100}$	$0.06152 + 0.1107i$	$0.06222 + 0.2850i$	$-0.2863 - 2.072i$
$\frac{2}{100}$	$0.03880 + 0.08620i$	$0.1548 + 0.2984i$	$-0.1014 - 0.8485i$
$\frac{3}{100}$	$0.01922 + 0.06936i$	$0.2485 + 0.3023i$	$0.1907 - 0.1181i$
$\frac{4}{100}$	$0.001802 + 0.05664i$	$0.3370 + 0.2998i$	$0.4826 + 0.3712i$
$\frac{5}{100}$	$-0.01399 + 0.04659i$	$0.4195 + 0.2924i$	$0.7541 + 0.7143i$
$\frac{6}{100}$	$-0.02848 + 0.03843i$	$0.4960 + 0.2815i$	$1.002 + 0.9578i$
$\frac{7}{100}$	$-0.04190 + 0.03170i$	$0.5669 + 0.2679i$	$1.225 + 1.129i$
$\frac{8}{100}$	$-0.05439 + 0.02609i$	$0.6325 + 0.2520i$	$1.425 + 1.244i$
$\frac{9}{100}$	$-0.06609 + 0.02138i$	$0.6933 + 0.2345i$	$1.604 + 1.314i$
$\frac{10}{100}$	$-0.07707 + 0.01741i$	$0.7494 + 0.2158i$	$1.761 + 1.348i$
$\frac{11}{100}$	$-0.08743 + 0.01406i$	$0.8012 + 0.1960i$	$1.899 + 1.351i$
$\frac{12}{100}$	$-0.09721 + 0.01124i$	$0.8489 + 0.1757i$	$2.017 + 1.328i$
$\frac{13}{100}$	$-0.1065 + 0.008874i$	$0.8927 + 0.1549i$	$2.115 + 1.284i$
$\frac{14}{100}$	$-0.1152 + 0.006897i$	$0.9328 + 0.1340i$	$2.195 + 1.220i$
$\frac{15}{100}$	$-0.1235 + 0.005260i$	$0.9694 + 0.1132i$	$2.256 + 1.139i$
$\frac{16}{100}$	$-0.1314 + 0.003918i$	$1.003 + 0.09278i$	$2.297 + 1.044i$
$\frac{17}{100}$	$-0.1389 + 0.002832i$	$1.033 + 0.07284i$	$2.318 + 0.9377i$
$\frac{18}{100}$	$-0.1460 + 0.001971i$	$1.060 + 0.05365i$	$2.319 + 0.8212i$
$\frac{19}{100}$	$-0.1528 + 0.001304i$	$1.084 + 0.03541i$	$2.299 + 0.6968i$
$\frac{20}{100}$	$-0.1592 + 0.0008049i$	$1.105 + 0.01837i$	$2.256 + 0.5670i$

Table 2: Dimensionless form factor $1000 \cdot \hat{B}$ of order α_s^2 for the operator O_2, given at the 23 points in Eq. (3.2). The three columns are the coefficients of ϵ^{-2}, ϵ^{-1} and ϵ^0, respectively. The value of the ϵ^{-3} coefficient is z-independent and is equal to 0.06073 for all points.
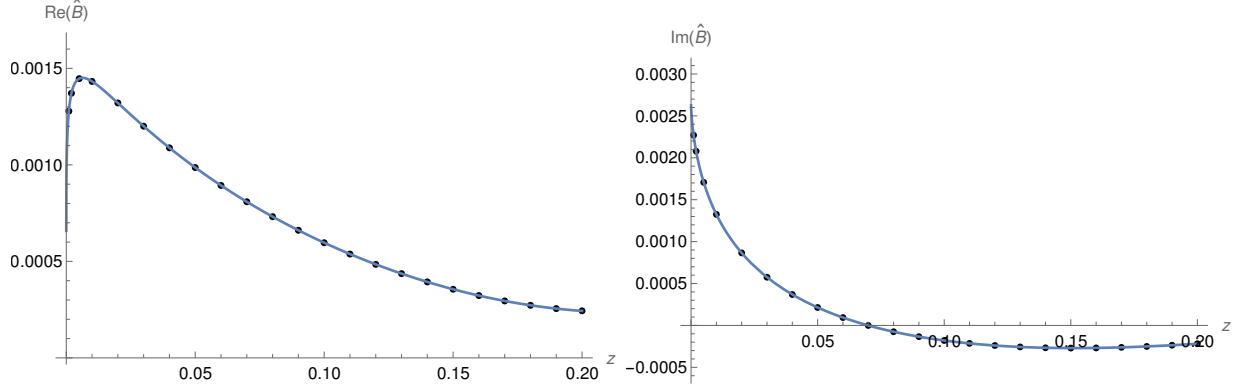
Figure 6: ϵ^0 coefficient of the O_1 contributions to $\hat{B}$ as defined in Eq. (4.1). The highlighted 23 points are mentioned in the text. The solid line is constructed by switching at $z = 0.04$ from the asymptotic expansion to the Taylor expansion.
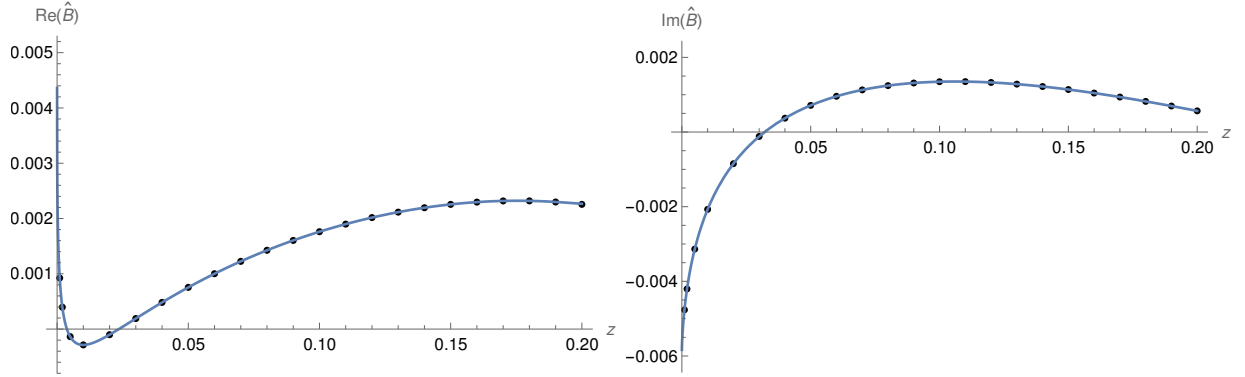

Figure 7: ϵ^0 coefficient of the O_2 contributions to $\hat{B}$ as defined in Eq. (4.1). The highlighted 23 points are mentioned in the text. The solid line is constructed by switching at $z = 0.04$ from the asymptotic expansion to the Taylor expansion.

which is in perfect agreement with our result. The main difference between our work and ref. [9] lies in the methods used: While they apply their "expand and match" approach as developed in [34–36] to construct the series expansions of the MIs, we directly utilize `DESolver` and `DiffExp` to generate the expansions around $z = 0$ and $z = 1/10$.

5   Summary

In this paper we worked out three-loop diagrams (of order α_s^2) contributing to the decay amplitude for $b \to s\gamma$ associated with the current-current operators O_1 and O_2 at different values of m_c. As a continuation of the work done in [8], we have calculated diagrams where at least one gluon is touching the b-quark line (see Figure 1 and Figure 2) in the present paper. We have also worked out all three-loop diagrams with bubbles on the gluon lines (see Figure 3). We have used `AMFlow` to calculate the boundary conditions for all diagrams at $z = 1/100$, as described in Section 3.1. Using these boundary conditions, we were able to calculate the results at 23 different points between $z = 1/1000$ and $z = 1/5$ with very high precision. We have also calculated the asymptotic expansion around $z = 0$ for all diagrams, which are useful in many practical applications. For the "b-leg diagrams", the asymptotic expansion breaks down at $z \sim 0.07$, therefore we also worked out a Taylor expansion around $z = 1/10$, which corresponds to the physical value. For most diagrams the same expressions have also been calculated using `DiffExp`, and the results using these two programs agree with very high precision. Our asymptotic expansions have been compared with the asymptotic expansions in [9], and we noticed very good agreement.

The numerical results at the 23 points in Eq. (3.2) are given for O_1 and O_2 in Tables 1 and 2, respectively. These results and the symbolic expression for the asymptotic formula up to z^{20} (as well as the symbolic expression for the Taylor expansion for the "b-leg diagrams" up to $(z - 1/10)^{20}$) are given in electronic form in the file `ancillary.m` which is submitted together with this paper.

Acknowledgements

A Details on the ancillary file

A.1 Results for the individual contributions of different diagram classes to the form factor $\hat{B}$ in electronic form

In the mathematica file "ancillary.m" (which is included in the submission of this paper) we give the contributions to the form factor $\hat{B}$ as defined in Eq. (4.1) for the 4 different classes of diagrams ("b-leg diagrams", "s-leg diagrams", "mixed diagrams" and "bubble diagrams").

All the results mentioned in the paper are given in this file. Firstly, the values at the 23 points in Eq. (3.2) are presented for all 4 classes of diagrams for both O_1 and O_2. For the O_1 contributions, these are the expressions `BlegPointsO1`, `SlegPointsO1`, `MixedPointsO1` and `BubblesPointsO1` for the 4 classes of diagrams, respectively (the same expressions for O_2 are named accordingly). The asymptotic expansions are also presented up to order z^{20} for all classes of diagrams. The corresponding expressions for O_1 are `BlegAsymO1`, `SlegAsymO1`, `MixedAsymO1` and `BubblesAsymO1`. As mentioned in the paper, the Taylor expansion around $z = 1/10$ is also presented for the "b-leg diagrams", as a function of u, where $u = z - 1/10$, up to order u^{20}. This expression for O_1 is `BlegTaylorO1`.

Note that these formulas contain the following symbolic constants: $nl = 3$ (number of 'light' quarks), $nb = 1$ (number of quarks with mass equal to m_b), $nc = 1$ (number of quarks with mass equal to m_c), $ca = 3, cf = 4/3, tr = 1/2$ (color factors), $Qd = -1/3$ (charge of down-type quark) and $Qu = 2/3$ (charge of up-type quark). All these constants are given in the ancillary file.

At the end of the ancillary file, we present the two functions `FormFactorBhatO1` and `FormFactorBhatO2`, which, for a given value of z, return the form factor $\hat{B}$ corresponding to all 4 classes of diagrams, with all the symbolic constants inserted, for O_1 and O_2, respectively. These functions automatically choose the correct expansion for the "b-leg diagrams" depending on whether the given value of z is larger than $z = 0.04$.

References

[1] M. Misiak et al., *Estimate of $\mathcal{B}(B \to X_s\gamma)$ at $O(\alpha_s^2)$*, Phys. Rev. Lett. 98 (2007) 022002 [arXiv:hep-ph/0609232 [hep-ph]].

[2] M. Misiak et al., *Updated NNLO QCD predictions for the weak radiative B-meson decays*, Phys. Rev. Lett. 114 (2015) 221801 [arXiv:1503.01789 [hep-ph]].

[3] Y. S. Amhis et al. [HFLAV], *Averages of b-hadron, c-hadron, and τ-lepton properties as of 20 21*; Phys. Rev. D 107 (2023), 052008 [arXiv:2206.07501 [hep-ex]].

[4] M. Misiak, A. Rehman, M. Steinhauser, *Towards $B \to X_s\gamma$ at the NNLO in QCD without interpolation in m_c*, JHEP 06 **175** (2020) [arXiv:2002.01548 [hep-ph]].

[5] Z. Ligeti, M.E. Luke, A.V. Manohar and M.B. Wise, *The $\bar{B} \to X_s\gamma$ photon spectrum*, Phys. Rev. D **60** (1999), [arXiv:hep-ph/9903305 [hep-ph]].

[6] K. Bieri, C. Greub and M. Steinhauser, *Fermionic NNLL corrections to $b \to s\gamma$*, Phys. Rev. D **67** (2003), 114019 [arXiv:hep-ph/0302051 [hep-ph]].

[7] R. Boughezal, M. Czakon and T. Schutzmeier, *NNLO fermionic corrections to the charm quark mass dependent matrix elements in $\bar{B} \to X_s\gamma$*, JHEP 09 **072** (2007), [arXiv:0707.3090 [hep-ph]].

[8] C. Greub, H.M. Asatrian, F. Saturnino, C. Wiegand *Specific three-loop contributions to $b \to s\gamma$ associated with the current-current operators*, JHEP 05 **201** (2023) [arXiv:2303.01714 [hep-ph]].

[9] M. Fael, F. Lange, K. Schönwald and M. Steinhauser *Three-loop $b \to s\gamma$ vertex with current-current operators*, JHEP 11 **166** (2023) [arXiv:2309.14706 [hep-ph]].

[10] M. Czaja, M. Czakon, T. Huber, M. Misiak, M. Niggetiedt, A. Rehman, K. Schönwald and M. Steinhauser, *The $Q_{1,2}$–Q_7 interference contributions to $b \to s\gamma$ at $\mathcal{O}(\alpha_s^2)$ for the physical value of m_c*, Eur. Phys. J. C **83** (2023) no.12, 1108 [arXiv:2309.14707 [hep-ph]].

[11] C. Greub, T. Hurth and D. Wyler, *Virtual $O(\alpha_s)$ corrections to the inclusive decay $b \to s\gamma$*, Phys. Rev. D **54** (1996), 3350-3364 [arXiv:hep-ph/9603404 [hep-ph]].

[12] I. R. Blokland, A. Czarnecki, M. Misiak, M. Slusarczyk and F. Tkachov, *The Electromagnetic dipole operator effect on $\bar{B} \to X_s\gamma$ at $O(\alpha_s^2)$*, Phys. Rev. D **72** (2005), 033014 [arXiv:hep-ph/0506055 [hep-ph]].

[13] H. M. Asatrian, T. Ewerth, A. Ferroglia, P. Gambino and C. Greub, *Magnetic dipole operator contributions to the photon energy spectrum in $\bar{B} \to X_s\gamma$ at $O(\alpha_s^2)$*, Nucl. Phys. B **762** (2007), 212-228 [arXiv:hep-ph/0607316 [hep-ph]].

[14] T. Muta, *Foundations Of Quantum Chromodynamics*, World Sci. Lect. Notes Phys. 5, 1 (1987).

[15] G. Buchalla, A. J. Buras and M. E. Lautenbacher, *Weak decays beyond leading logarithms*, Rev. Mod. Phys. **68**, 1125 (1996) [hep-ph/9512380].

[16] J. Aebischer, M. Fael, C. Greub and J. Virto, *B physics Beyond the Standard Model at One Loop: Complete Renormalization Group Evolution below the Electroweak Scale*, JHEP 09, **158** (2017) [arXiv:1704.06639 [hep-ph]].

[17] M.E. Peskin and D.V. Schroeder, *An Introduction to Quantum Field Theory*, Addison-Wesley Publishing Company, (1995).

[18] J. Klappert, F. Lange, P. Maierhöfer and J. Usovitsch, *Integral reduction with Kira 2.0 and finite field methods*, Comput. Phys. Commun. **266** (2021), 108024 [arXiv:2008.06494 [hep-ph]].

[19] P. Maierhöfer, J. Usovitsch and P. Uwer, *Kira—A Feynman integral reduction program*, Comput. Phys. Commun. **230** (2018), 99-112 [arXiv:1705.05610 [hep-ph]].

[20] R. H. Lewis, *Computer Algebra System Fermat*, https://home.bway.net/lewis

[21] J. Klappert, S. Y. Klein and F. Lange, *Interpolation of dense and sparse rational functions and other improvements in FireFly*, Comput. Phys. Commun. **264** (2021), 107968 [arXiv:2004.01463 [cs.MS]].

[22] J. Klappert and F. Lange, *Reconstructing rational functions with FireFly*, Comput. Phys. Commun. **247** (2020), 106951 [arXiv:1904.00009 [cs.SC]].

[23] J. Usovitsch, *Factorization of denominators in integration-by-parts reductions*, [arXiv:2002.08173 [hep-ph]].

[24] S. Laporta, *High precision calculation of multiloop Feynman integrals by difference equations*, Int. J. Mod. Phys. A **15** (2000), 5087-5159 [arXiv:hep-ph/0102033 [hep-ph]].

[25] R. N. Lee, *Presenting LiteRed: a tool for the Loop InTEgrals REDuction*, arXiv:1212.2685 [hep-ph].

[26] R. N. Lee, *LiteRed 1.4: a powerful tool for reduction of multiloop integrals*, J. Phys. Conf. Ser. **523** (2014), 012059 [arXiv:1310.1145 [hep-ph]].

[27] C. Meyer, *Algorithmic transformation of multi-loop master integrals to a canonical basis with CANONICA*, Comput. Phys. Commun. **222**, 295 (2018) [arXiv:1705.06252 [hep-ph]].

[28] A. B. Goncharov, *Multiple polylogarithms, cyclotomy and modular complexes*, Math. Res. Lett. **5**, 497 (1998) [arXiv:1105.2076 [math.AG]].

[29] R. N. Lee, *Libra: A package for transformation of differential systems for multiloop integrals*, Comput. Phys. Commun. **267** (2021), 108058 [arXiv:2012.00279 [hep-ph]].

[30] A. V. Smirnov, N. D. Shapurov and L. I. Vysotsky, *FIESTA5: Numerical high-performance Feynman integral evaluation*, Comput. Phys. Commun. **277** (2022), 108386 [arXiv:2110.11660 [hep-ph]].

[31] X. Liu and Y. Q. Ma, *AMFlow: A Mathematica package for Feynman integrals computation via auxiliary mass flow*, Comput. Phys. Commun. **283**, 108565 (2023) [arXiv:2201.11669 [hep-ph]].

[32] X. Liu, Y. Q. Ma and C. Y. Wang, *A Systematic and Efficient Method to Compute Multiloop Master Integrals*, Phys. Lett. B **779** (2018), 353-357 [arXiv:1711.09572 [hep-ph]].

[33] M. Hidding, *DiffExp, a Mathematica package for computing Feynman integrals in terms of one-dimensional series expansions*, Comput. Phys. Commun. **269**, 108125 (2021) [arXiv:2006.05510 [hep-ph]].

[34] M. Fael, F. Lange, K. Schönwald and M. Steinhauser, *A semi-analytic method to compute Feynman integrals applied to four-loop corrections to the $\overline{\text{MS}}$-pole quark mass relation*, JHEP **09** (2021), 152 [arXiv:2106.05296 [hep-ph]].

[35] M. Fael, F. Lange, K. Schönwald and M. Steinhauser, *Massive Vector Form Factors to Three Loops*, Phys. Rev. Lett. **128** (2022) no.17, 172003 [arXiv:2202.05276 [hep-ph]].

[36] M. Fael, F. Lange, K. Schönwald and M. Steinhauser, *Singlet and nonsinglet three-loop massive form factors*, Phys. Rev. D **106** (2022) no.3, 034029 [arXiv:2207.00027 [hep-ph]].